Article

Effects of Viscosity and Salt Interference for Planar Iridium Oxide and Silver Chloride pH Sensing Electrodes on Flexible Substrate

Khengdauliu Chawang [ID], Sen Bing [ID] and Jung-Chih Chiao *[ID]

Electrical and Computer Engineering, Southern Methodist University, Dallas, TX 75205, USA
* Correspondence: jchiao@smu.edu

Abstract: The equivalency of pH measurements between aqueous and non-aqueous or viscous solutions is of great interest in biomedical applications as well for processing food and pharmaceuticals. Commercial glass-type electrodes have practical limitations, such as bulky sizes and membrane clogging in viscous environments. In this study, planar and flexible electrochemical pH sensors with iridium oxide as the sensing film have been developed by sol-gel and oxidation processes. A reference electrode was prepared by screen printing Ag/AgCl ink on the same polyimide substrate. The small form factors of the planar flexible electrodes provide an advantage in small volume or conformal surface measurements. Cyclic voltammetry was performed in different pH solutions. The electrode originally produced a response of −70.1 mV/pH at room temperature in aqueous solutions. The sensitivities were reduced when salt was added into the buffer solutions, although output potentials were increased. Sensing performances in a wide range of viscous conditions with various concentrations of added salt have been analyzed to study their effects on pH-sensing responses. Suitable calibration techniques using aqueous buffer solutions were studied for output potentials and their respective pH readings in viscous salt-added solutions. The mechanisms affecting output potentials are explained and results matched well for two different thickening agents. Specificity to pH changes measured by the planar IrO_x-Ag/AgCl pH electrodes showed how the potential-pH calibration should consider the interference effect of salt. The viscosity effects on pH reading errors became more pronounced as solution viscosity increased. Comparisons of pH readings to those from a commercial glass-bodied pH meter indicated that the planar electrodes provided predictable pH deviations that were confined to a limited range. The planar IrO_x-Ag/AgCl electrodes on flexible polyimide substrates have mostly been demonstrated with aqueous solutions in various diagnostic and environmental monitoring applications. This work provides more insights into pH sensing performance when the fluid is viscous and contains salt, which often is the case in biomedical and food-processing applications.

Keywords: pH sensor; salt interference; viscosity; flexible; calibration

1. Introduction

Measuring the pH of viscous and non-aqueous solutions is of great importance in applied chemistry applications [1–3] such as in processing food [4,5], cosmetics [6,7], and pharmaceuticals [8,9]. The pH sensing mechanism involved in the aqueous solution is well established; however, studies in non-aqueous or viscous solutions have been limited. Some common issues faced using conventional glass-rod pH sensors are slow responses, frequent calibration, and glass membrane clogging and corrosion in the inner electrolyte, which limits their use in non-aqueous solutions. K. Izutsu et al. demonstrated slow responses of glass pH electrodes in a non-aqueous solvent tested in an acid-based titration method [2]. For reliable pH measurements, J. F. Artiola reported the need for frequent two-/three-point calibrations with periodic glass membrane soaking in a standard solution to remove organic

salts [10]. The literature also suggests that the dissociation of functional groups on glass body surfaces may decrease Nernstian responses [11]. The traditional bulky glass-rod shaped pH sensors cannot be used for sensing a small volume of liquid or on planar surfaces. Owing to their features of miniaturization, integration with electronics, and the elimination of membranes, planar solid-state films have been proposed for pH sensing electrode materials [12–14].

Among metal oxides, iridium oxide (IrO_x) based films have been studied to exhibit higher Nernstian responses [15], reproducible super-Nernstian responses within wide pH ranges in aqueous solutions [16], and faster responses in non-aqueous solutions compared to commercial pH meters [2]. Stable pH-sensing performance after exposure to high temperatures and their biocompatibility feature was reported in the literature [17,18]. IrO_x films have been studied for use in implantable devices and cochlear prostheses [19–21]. Fabrication methods for iridium oxide films by radio-frequency (RF) sputtering [22,23], electroplating [24–26], chemical bath [27,28], and sol-gel deposition with oxidation have been conducted [29–31]. These methods are chosen according to the device and production requirements. The sol-gel method provides advantages for mass production, fabrication simplicity, and lower costs. Deposition through dipping in sol-gel solutions has been used in industrial manufacturing processes. It can be applied to a wide variety of substrates. Iridium oxide (IrO_x) based pH sensors on flexible substrates made by the sol-gel method have been demonstrated in the following ways: with Nernstian responses [32], in an array configuration [33], integrated with other chemical sensors [34], and for food-quality and medical implant applications [35–37]. In these demonstrations, planar IrO_x working electrodes integrated with Ag/AgCl reference electrodes were calibrated and tested in aqueous conditions with and without interfering salt effects.

Salt addition in an aqueous pH solution was demonstrated to have interfering effects on the potential and pH outputs previously demonstrated using planar electrodes in our group [34]. In this study, we explored the effects of ionic interferences from salt (NaCl), and viscosity on planar IrO_x and Ag/AgCl electrode potential outputs. Aqueous pH solutions were used as the calibration standard to estimate the pH values of viscous salt-added solutions. Solutions with different pH values, NaCl concentrations, and viscosities, which varied by adding thickening agents, were prepared. In each configuration of the solution, three pairs of planar IrO_x and Ag/AgCl electrodes were used to investigate performance variations.

We proposed planar pH electrodes under the consideration of the practical constraints faced when using glass-rod membrane-based sensors in viscous solutions. Preliminary results of using the planar electrodes were submitted and accepted to present at the 2022 IEEE Sensors Conference [38]. In this study, details of the investigation and experimental results for the effects of salt and viscosity on potential and pH outputs are reported.

Planar pH sensors were prepared, each consisting of an IrO_x working electrode (WE) and an Ag/AgCl reference electrode (RE) on a biocompatible, inert, and flexible polyimide substrate [38]. IrO_x was deposited as the H^+ ion sensing film by the sol-gel and oxidation processes. Ag/AgCl film was deposited by screen printing on the flexible substrate. The monolithic processes allowed miniaturization without the need for a vacuum environment. A commercial Ag/AgCl glass-rod electrode was used for calibration in aqueous pH buffer solutions, but could not be reliably used in viscosity experiments because of its dependency on ion migration to remain stable [10]. In a non-aqueous interface, the liquid junction potential may become large and unreliable. The planar electrodes, on the contrary, allow direct surface contact with the viscous solution samples.

2. Materials and Tools

Technical grade Iridium (IV) Chloride ($IrCl_4$) hydrate powder (Sigma Aldrich, Saint Louis, MO, USA) was used to prepare the sol-gel solution for WE. Ethyl Alcohol 200 Proof (Supelco, Bellefonte, PA, USA) was used during the preparation of the sol-gel solution. Glacial acetic acid (Fisher Scientific, Waltham, MA, USA) with 99.7% concentration was used as the

reagent. To prepare the reference electrode, Ag/AgCl paste (011464, ALS, Kanagawa, Japan) was used. Electrical connections between electrodes and the interface were made of copper wires and adhesive silver epoxy (8331D, MG Chemicals, USA).

Different viscosities of the solution were achieved by adding thickening agents into pH solutions. Lab graded starch powder $(C_6H_{10}O_5)_n$ (Carolina Biological Supply Company, Burlington, NC, USA), and agar powder $C_{14}H_{24}O_9$ (Seaweed Solution, Trondheim, Norway), which is a and natural gelatin were used as the thickening agents. DI water with a conductivity of 0.055 μS/cm at room temperature was used for experiments. Hydrochloric acid (HCl) (LabChem, Zelienople, PA, USA) with a concentration of 50% was mixed with DI water to adjust the pH level to 4. The reason for the preparation of the custom-made pH 4 solution with HCl was to investigate interference from other ionic elements because commercial buffer solutions contained various chemicals. Similarly, custom-made pH 6 and pH 8 solutions were prepared with HCl and sodium hydroxide (NaOH) (Sigma Aldrich, MO, USA) in DI water. A commercial pH meter (A1311, Apera Instruments, Columbus, OH, USA) and pH/conductivity benchtop multiparameter (Orion Star A215, Thermo Fisher Scientific, Waltham, MA, USA) were used to adjust and verify the pH levels in aqueous solutions. The same benchtop multiparameter was used to measure the conductivity of aqueous solutions. Commercial buffer pH 4, 6, and 8 solutions (Fisher Scientific, MA, USA) were also used for experiments. Lab-grade sodium chloride (NaCl) (Macron, PA, USA) was added to the pH solutions after the thickening agents, which allowed for the study of ionic interferences to the sensing electrodes in viscous environments. Different viscous samples were prepared at the same time and stored in 50-mL plastic storage vials. Multiple viscometers were used including a modified Ostwald viscometer (CANNON Instrument Company, PA, USA), a rheometer (HR-3, TA Instruments, MN, USA), and a digital viscometer (KUNHEWUHUA, China). These meters together covered a wider range of viscosity. A data acquisition card (National Instruments 6201, USA) was used for signal recording.

3. Experiments

3.1. Electrode Preparation

Both the working electrode (WE) and reference electrode (RE) were prepared on a flexible polyimide substrate with a 125-μm thickness (500HN, Dupont, Newark, DE, USA). The WE consisted of two metal layers: gold (Au) and chromium (Cr), both deposited by electron-beam evaporation. Cr was used as an adhesion layer with a thickness of 50 nm. Au as the base metal layer had a thickness of 200 nm. IrO_x serving as the sensing film was deposited on Au by the sol-gel dipping process. The sol-gel solution was prepared by mixing 1 g of anhydrous $IrCl_4$ with 42 mL of 200 Proof alcohol, and 10 mL of 80% concentrated acetic acid was later added. Using a magnetic stirrer set at 500 rpm, the solution was mixed for 2 h at 25 °C before use.

The substrate with base metal was coated by dipping and was dried at 50 °C. The dipping and drying processes were repeated three times. Then, samples were heated for 4 h at 325 °C [39–41]. To prepare RE, a layer of Ag/AgCl paste was applied to the substrate and dried at 120 °C. Both WE and RE films were cut into strips of 2 mm × 15 mm and fixed with a spacing distance of 3 mm between the two electrodes.

3.2. Viscous Sample Preparation

Starch solutions with different concentrations (wt%) were prepared in beakers. Three types of solutions were used for tests at pH 4, 6, and 8. The solution for pH 4 was prepared by mixing DI water and HCl, and the solutions for pH 6 and 8 were commercial buffer solutions. The solution was heated in a beaker and starch was added at a boiling temperature (95 °C). Magnetic stirring was performed at 500 rpm for 20 min until aggregation of starch powders disappeared in the solutions.

After the starch powder was completely dissolved in the solution, salt was added, and stirring continued for 5 min in the hot solution. Similarly, agar-based viscous solutions were

also prepared. A total of 183 different variations of viscous samples, including 165 starch-based and 18 agar-based solutions, were prepared. Each test vial contained a 50 mL solution with a specific viscosity, pH value, and salt concentration. Output potential recordings were performed at room temperature.

4. Results and Discussion

4.1. Cyclic Voltammetry Analysis

Electrochemical studies on the polyimide-based WE and RE were investigated using cyclic voltammetry (CV) analysis performed in aqueous pH solutions. Figure 1a shows the CV comparison in pH 4 solution without salt and with 1-M NaCl salt. The broader curves during cathodic and anodic scans were due to higher currents generated with conducting salt ions. Figure 1b compares CV curves of pH 4, 6, and 8 with 1-M NaCl salt added. The pH 4 solution only contained HCl, while the buffer pH 6 solution had sodium hydroxide (NaOH) and dihydrogen potassium phosphate (KH_2PO_4) groups; thiomersal ($C_9H_9HgNaO_2S$), NaOH, and KH_2PO_4 groups were in the pH 8 buffer solution. The additional conducting ions in the buffer pH 6 and pH 8 solutions generated higher currents and produced broader voltammograms. The CV analysis provided certainty that such planar electrodes could be used to generate sufficient potentials and currents in various pH solutions.
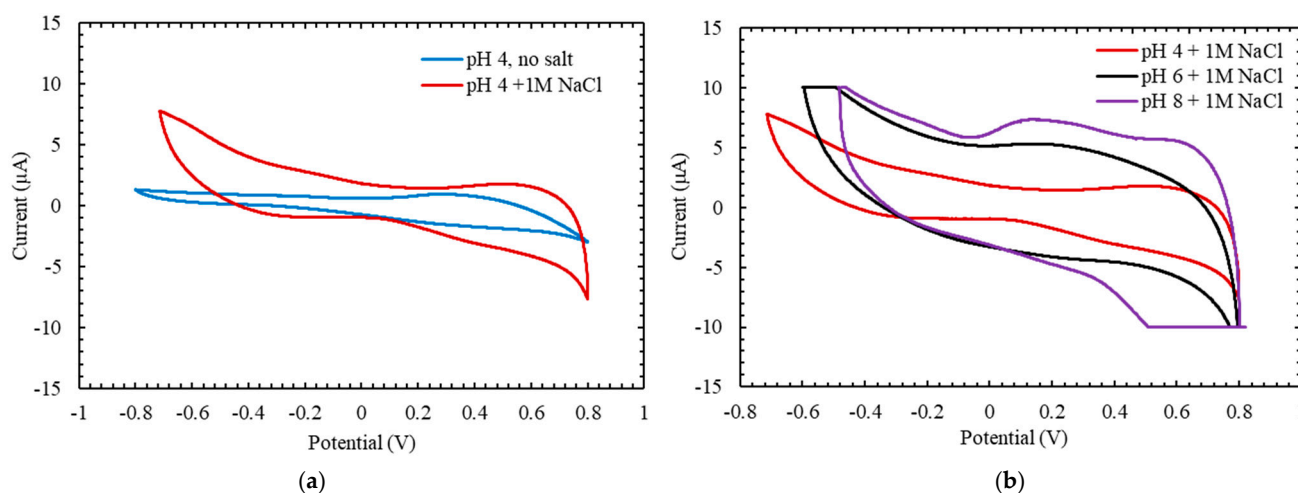

Figure 1. Cyclic voltammetry (CV) comparison of (**a**) pH 4 aqueous solution without salt (0 M) and 1-M NaCl salt added; and (**b**) pH 4, pH 6, and pH 8 aqueous solutions with 1-M NaCl salt added.

4.2. Nernstian Response in Aqueous Solutions

The ion exchanges on the working electrode (WE) surfaces created a potential difference against the reference electrode (RE) across the solution volume. Under ideal conditions without ionic or hydrodynamic interferences at room temperature, the Nernstian response in an aqueous solution should be around −59 mV/pH, as demonstrated in previous works [31–33].

Figure 2 compares the pH potential responses with no salt, 0.1-M, and 1-M NaCl salt added in aqueous pH 4, 6, and 8 solutions. A super-Nernstian response of −70.1 mV/pH was measured without salt added in the buffer solutions. Redox mechanisms for IrO_x producing Nernstian or super-Nernstian responses were explained in the literature [41–45]. Compared to our previous results, a possible explanation for the super-Nernstian response was that a controlled fabrication process was implemented. The WEs were prepared by multiple repeated steps of dip-coating and drying processes to achieve uniform thickness. The REs were prepared by screen printing commercial Ag/AgCl ink on the substrate instead of electroplating [38]. The sensitivity in the no-salt case decreased to near-Nernstian responses of −53.3 mV/pH when 0.1-M salt was added, and −47.3 mV/pH when 1-M NaCl was added. Increased output potentials were due to increased solution conductivities

by salt ions. However, the output potential increased more in the alkaline solution as soon as salt was added. The decreased sensitivity validated that interference from salt ions existed.
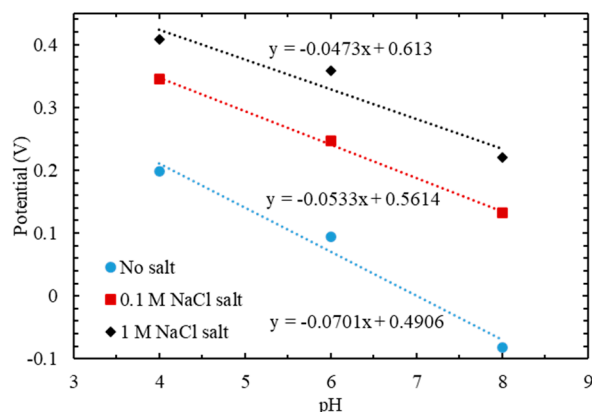

Figure 2. Sensitivities for aqueous no-salt (0 M), 0.1-M, and 1-M NaCl salt concentrations, calibrated at pH 4, 6, and 8 solutions.

To validate the effect of salt interference, the same solutions were measured by a glass-bodied pH meter. Figure 3a–c show pH and conductivity changes as salt was added to the pH 4, 6, and 8 solutions. The pH and conductivity were measured by a commercial pH/conductivity meter (Orion, A215). The addition of salt increased solution conductivity and made the solution seem more acidic. This effect decreased the output pH values calculated by the calibration curve obtained with standard calibration buffers. At 0.1-M salt concentrations, the pH values shifted to 4.01, 5.81, and 7.8 from their respective values of 4, 6, and 8. At 1-M salt concentrations, the values became 3.88, 5.2, and 7.4.
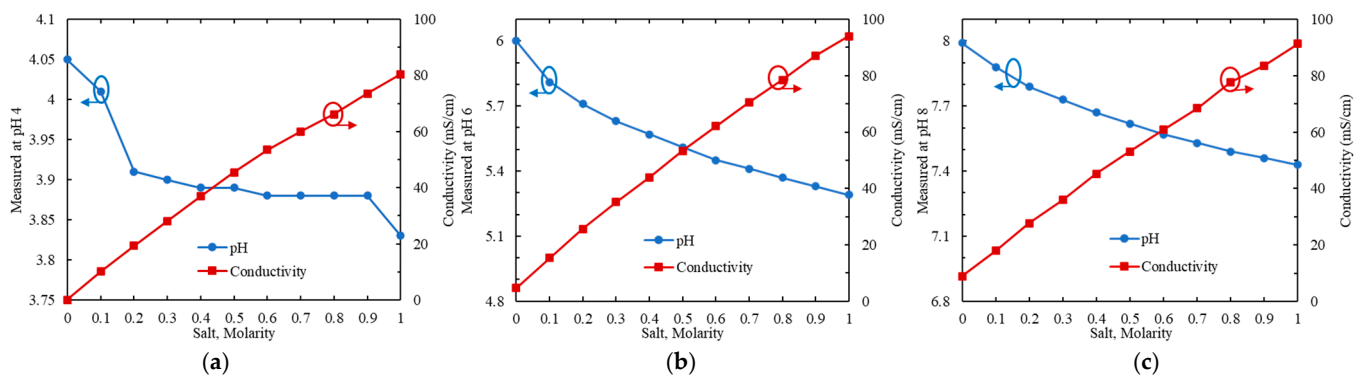

Figure 3. Measured pH and conductivity changes after 0.1–1 M NaCl salt addition in (**a**) pH 4, (**b**) pH 6, and (**c**) pH 8 aqueous solutions.

4.3. Viscosity Readings

Different percentages by weight, listed in Table 1, of starch and agar as thickening agents were prepared with no salt or salt added to achieve certain viscosities. Although the concentrations of the starch by weight varied from 1% to 4%, and 0.05% to 0.2% for agar, the viscosities varied quite significantly. Three different types of viscometers were used to validate the fluid viscosity because of their respective detection limitations.

An Ostwald viscometer was used to measure the viscosity of the starch sample with the lowest concentration of 1%. A rheometer for the concentration ranging from 1.0% to 2.0%, and a digital viscometer for 1.8% to 4.0% were used. For starch concentrations of 1.8% and 2.0%, both meters were used to cross-validate their viscosity values. The digital viscometer was used to measure agar samples since the viscosities were high. Agar solution

with a concentration beyond 0.2% could not be measured by viscometers because it became a gel-like solid.

Table 1. Viscosity readings.

Thickening Agent	wt%	Viscosity (cP)
Starch	1	1.17
	1.4	2.39
	1.8	24
	2	47
	3	135
	4	820
Agar	0.05	54
	0.1	360
	0.2	2553

4.4. Experiments with Starch as the Thickening Agent

All experiments were performed by immersing the electrode area into the viscous solution samples. Electrodes were tested at pH 4, 6, and 8 solutions mixed with different NaCl concentrations (0–1 M with/without starch or agar). Output potential was recorded for 17 s and the electrodes were cleaned in deionized (DI) water for 30 s to remove residue from surfaces.

The custom-made pH 4 solution had a conductivity of 120 μS/cm. For weak acid and alkaline, the conductivities of custom-made pH 6 and 8 solutions mixing DI water with HCl or NaOH were 47 and 27 μS/cm, respectively. Unstable readings were observed for pH 6 and pH 8 cases. To overcome the issue, likely due to low conductivity, commercial buffer solutions at pH 6 and 8 with conductivities of 4726 and 8460 μS/cm were used instead. As mentioned previously during the CV analysis, various conducting ions were present in buffer pH 6 and 8 solutions, and it was expected that the additional ions in the solutions might create interfering effects.

Figure 4 shows the measured potentials in the starch-based measurements with (a) no salt and (b) 1-M NaCl salt added. The outputs in time stayed stable without significant drifts. Some fluctuation in signals might be due to liquid motions in beakers. Although other salt concentrations were also tested, only no-salt and 1-M salt cases are shown for illustration purposes. The five colors indicate 0%, 1%, 2%, 3%, and 4% starch added, with viscosities of 0.89, 1.17, 47, 135, and 820 cP, respectively.
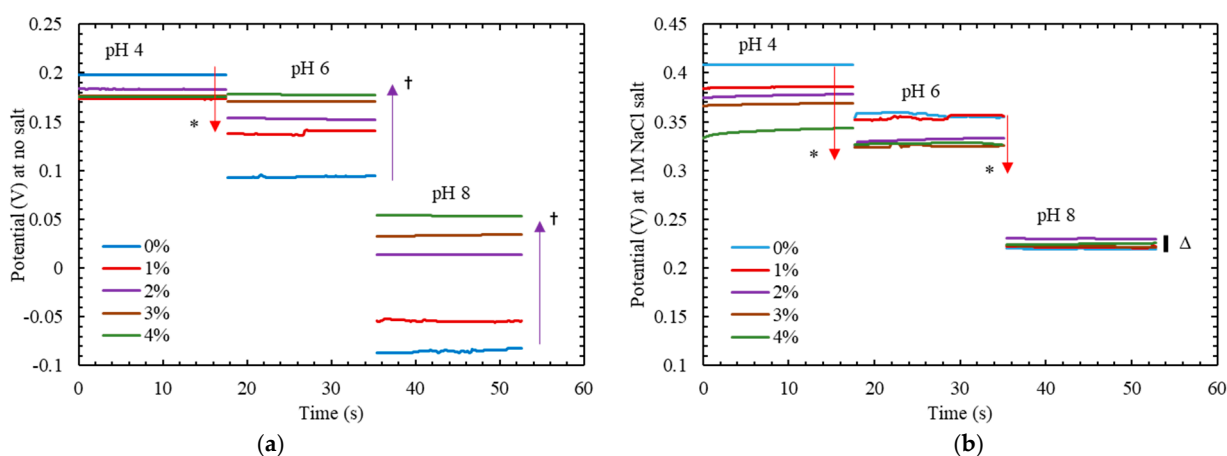

Figure 4. Output potentials in viscous starch-based solutions at pH 4, 6, and 8 for (a) no salt added and (b) 1 M salt concentration. The symbols * and † indicate a monotonic decrease and increase as viscosity increases. The symbol Δ indicates no drastic change in output potentials as viscosity increases.

The arrows in Figure 4a,b indicate the decreasing (red) or increasing (purple) trends in potentials as starch concentration increases. When starch is heated above 90 °C, granules swell and release ionic species known as branched amylopectin and linear amylose into the solution [46,47]. Branched amylopectin is responsible for aggregation and creates viscous matrices, while linear amylose increases solution conductivity [48]. Electrochemical impedance spectroscopy (EIS) showed that, after starch gelatinization, electrical resistance in the viscous matrix was created by amylopectin which was an insoluble material [46]. In the no salt added case in Figure 4a, pH 4 has a higher H^+ concentration with the free flow of electrons from the redox equilibrium. The viscous matrices in high ionic concentration played a significant role and increased the electrical resistance that constrained the movements of free ions. The potential drop in the solution increased, which caused the measured voltage across the electrodes to decrease. Amylose in starch counteracted to decrease the solution resistance with additional electrons. The effects of amylose and matrices negated each other, so the potential decreased with smaller steps as the starch concentration increased. At lesser H^+ concentrations in pH 6 and 8, the effect from matrices to constrain flows of ions was less significant. Thus, the role of amylose became more pronounced in decreasing resistance in the solution, and potential increased with bigger steps as the starch concentration increased (purple arrow).

When salt was added, free flows of conductive ions significantly increased, and potentials at pH 4, 6, and 8 increased with significant steps. The matrices of amylopectin could constrain the ionic movements of salt. Compared to amylose, the salt provided more impact on conductivity increases, thus the amylose effect became less obvious. In return, the potential decreases at pH 4 (red arrow, Figure 4b) became more prominent as the viscosity increased. Compared to Figure 4a, the electrical resistance in the solution increased more when its viscosity increased. For the same reason, the constraining effect of matrices became more on free salt ions that overpowered the increased conductivity by amylose. As a result, Figure 4b shows that there was almost no change of potential at pH 8 for different viscosities. The negating effect was more obvious for pH 6 solutions comparing the opposite directions of the purple and red arrows in Figure 4a,b. When there was no salt added, the effect from amylose made the potential increase with increasing viscosities as conductivities increased. However, the abundant ions from adding salt were constrained by amylopectin matrices, which allows for the potential decrease when increasing viscosities. The potential decreases are shown in two steps in Figure 4b, instead of the multiple steps for pH 6 and 8 solutions in Figure 4a, because the negating effects were not linear or equal. It should also be noted that the viscosities for 1% and 2% starch concentrations were 1.17 and 47 cP, respectively, with a 40x increase, while the increase was 2.9 and 6 times from 47 to 135 cP and from 135 to 820 cP for the starch concentration increasing from 2% to 3% and 3% to 4%, respectively.

Figure 5a–c shows the comprehensive data of output potentials with different salt concentrations and starch percentages (at different viscosities) in solutions. Three electrode pairs were tested under the same protocol from no salt (0 M) to 1-M salt concentration with a step change of 0.1 M before they were switched to another viscosity. The decreasing trends of potentials when the viscosity increased at pH 4 and the increasing trends at pH 8 validated the results in Figure 4. For pH 6 without salt added, the potential increased when the viscosity increased. With salt added, the potential decreased when viscosity increased. The upward arrow at pH 4, 6, and 8 shows output potential monotonically increases as more salt is added to the aqueous or viscous solutions. The data matched well with those in Figure 4. From the aqueous solutions to cases with starch added, the potential differences were much larger at pH 6 and 8 because amylose provides more electrical currents in the solutions. Generally speaking, when NaCl was added, even as low as the 0.1 M concentration, the effects from the starch molecule matrices, which reduced conductivity, were not as effective as the increasing conductivity effect by adding salt ions. Potential changes had smaller steps for the salt-added cases when viscosities changed, compared to the potential jumps from the no-salt cases.
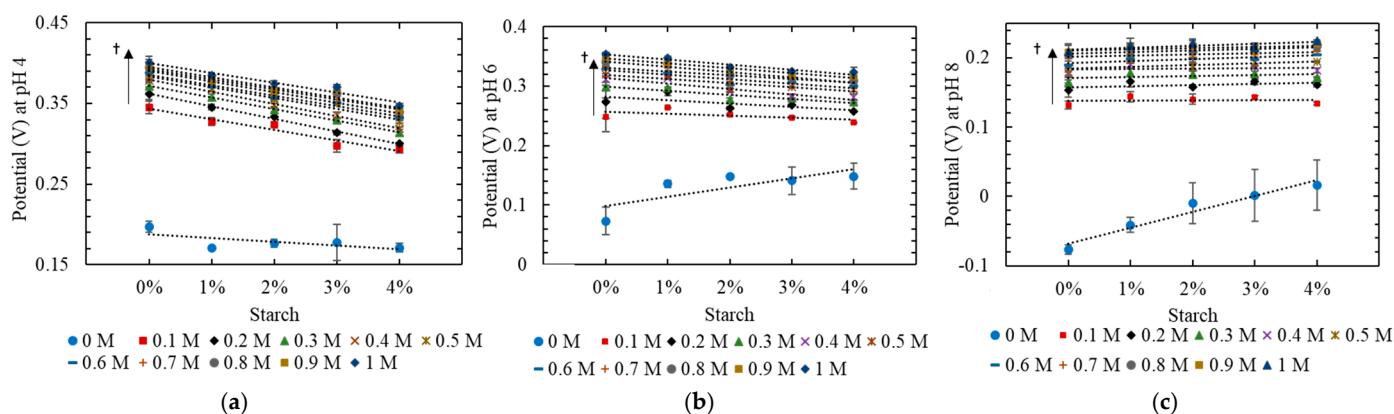
Figure 5. Measured output potential using starch as a thickening agent from 0–4% and salt 0–1 M added to (**a**) pH 4, (**b**) pH 6, and (**c**) pH 8 solutions. Error bars at every pH are the standard deviation of three sensors (n = 3). The † symbol indicates potential increases monotonically when 0.1–1 M NaCl salt is added.

The error bars in the plots of Figure 5 indicate the standard deviations measured by three sensors separately. The standard deviations in general were higher in solutions with higher viscosities when no salt was added to the solutions, particularly for the pH 8 cases. This might be due to the ions from amylose in viscous solutions, which were not uniform in the beakers, and the electrodes not experiencing more pronounced electrical current variations.

4.5. Experiments with Agar as the Thickening Agent

The experimental setup and procedure using agar powder as the thickening agent were similar to the starch-based experiments. Solutions were prepared with the custom-made pH 4 solution, and commercial pH 6 and 8 buffer solutions were also similar to the starch-based solutions. Each pH level had salt concentrations of 0 and 1 M, and three different viscosity levels.

Figure 6a,b show the results for agar-based measurements in which the three colors indicate 0%, 0.2%, and 0.6% agar added. The viscosity for 0.2% agar was measured as 2553 cP. When more than 0.2% agar was added to the solution, the viscometer could not receive a reading because the solution became gel-like. The electrodes could still be inserted into the gel, but it was obvious that they experienced mechanical resistance. Measurement results in the (a) no-salt condition are compared to those of (b) 1-M salt concentrations in Figure 6. Without added salt, a decreasing trend (red arrow) of potentials at pH 4 and increasing trends (purple arrow) at pH 6 and 8 were observed, as in Figure 6a. With 1-M salt added, the potentials stayed roughly in the similar levels at pH 4 and 8. The overall trend also showed decreased potentials when the viscosity increased. The trends for both no-salt and salt-added cases agreed with the starch-based cases in Figure 4. Although there is no report of ionic species contributed by agar, literature reported the conductivity of agar prepared with DI water was 73 µS/cm at 0.89% concentration [49]. The matrices and conductivity effects thus play similar roles to those in the starch-based solutions.

At pH 4 (red arrow, Figure 6a), the viscous matrices restricted flows of ions and increased the electrical resistance in the solution, which led to decreased output potentials. The potentials remained similar for 0.2% and 0.6% agar concentrations because these solutions have become very viscous. Most of the free-moving ions were constrained by the matrices. In Figure 6b, at pH 6 with salt added, there was the same phenomenon of a step drop of potential from 0% to 0.2% agar concentration, but no drop from 0.2% to 0.4% because most of the free ions from salt have been constrained at 0.2%. Increased potentials were observed (purple arrows in Figure 6a) at pH 6 and 8. Without added salt, low currents in low H^+ concentrations increased the conductivities with Agar, which reduced the potential drop in the solution and increased the potential between electrodes.
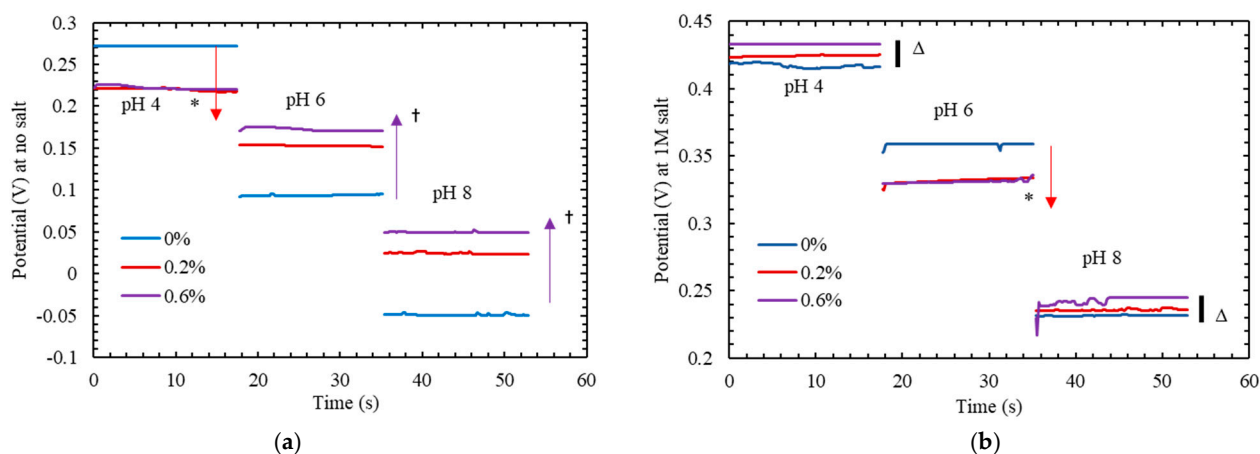
Figure 6. Output potentials in viscous agar solutions at pH 4, 6, and 8 for (**a**) no salt and (**b**) 1-M NaCl salt concentration. The symbols * and † indicate a monotonic decrease and increase as viscosity increases. The symbol Δ indicates no drastic change in output potential as viscosity increases.

When 1-M salt was added, the conductivities were dominated by the salt ions. Thus the additional conductivity from Agar of 73 µS/cm [49] did not play a significant role, which was much lower compared to 86.7 mS/cm from salt. The trend of pH 6 in Figure 6b with increasing viscosities was similar to the one in Figure 4b. The increasing trends at pH 4 and 8 were observed, but with smaller changes. Due to the high viscosity already at 0.2% agar concentration, conductivities in the solutions did not vary much.

In all tests, conductivity in the solution has been observed to play a role. The viscous matrix created by starch or agar change the potential output depending on initial ionic concentrations. The multifaceted mechanisms of conductivity and viscosity seem to counteract their effects in high ionic concentrations.

4.6. pH Calibration

The aforementioned measurements showed changes in output potentials under the influences of viscosity and salt concentrations. To illustrate the viscosity effect on pH reading, 2% and 4% viscous starch-based solutions, corresponding to viscosities 47 and 820 cP, were considered. With salt added, it was clear from previous results that the potentials could be significantly increased due to higher conductivities. Thus, pH reading errors may rise differently with respect to salt contents in solutions. We considered two scenarios for using three-point calibration curves at (1) unknown or (2) known salt concentrations in aqueous solutions. The pH values in solutions with different salt concentrations and viscosities were then calculated from the calibration curves.

Figure 7 demonstrates erroneous pH values when the calibration was conducted without knowing salt concentrations. The potential-pH relationship was first found in aqueous pH 4, 6, and 8 solutions without added salt. A sensitivity slope of -68.4 mV/pH was found and was used to convert the potentials generated in the viscous solutions (2% and 4% starch) to pH values. The initial pH values of 4, 6, and 8 were calculated as 2.2, 3.3, and 4.96 at 0.1-M salt cases, and 1.48, 2.03, and 3.76 at 1-M salt cases. The error bar in each salt concentration indicates the pH deviations at 2% and 4% starch concentrations from the aqueous conditions. The calibration clearly generated significant pH errors with the existence of salt and viscosity when the sensor calibration curve was produced without knowing salt concentrations.

The second calibration method was conducted at a known salt concentration. The three-point calibration was conducted at aqueous pH 4, 6, and 8 with known salt concentrations. For each salt concentration between 0.1 and 1 M, an individual sensitivity slope was generated. Then potentials in viscous starch solutions with different salt concentrations were converted to pH values. Figure 8 shows the results. The pH values calculated for the

viscous and salt-added pH 6 and 8 cases significantly improved with more accurate pH values. For example, the pH values for the pH 6 cases were 5.8 and 6.05 at 2% and 4% starch, respectively, at the 0.1-M salt concentration. Similarly, the pH values for the pH 8 cases were 7.9 and 8.01 at 2% and 4% starch, respectively, at the 0.1-M salt concentration. For comparison, the pH values measured by a commercial pH meter (A1311, Apera) for the pH 6 cases were 5.76 and 5.66 at 2% and 4% starch, respectively, at the 0.1-M salt concentration. For the pH 8 cases, the commercial pH meter readings were 7.32 and 7.79 at 2% and 4% starch at the 0.1-M salt concentration, respectively. Improvements in pH errors were also observed at other salt concentrations in Figure 8.
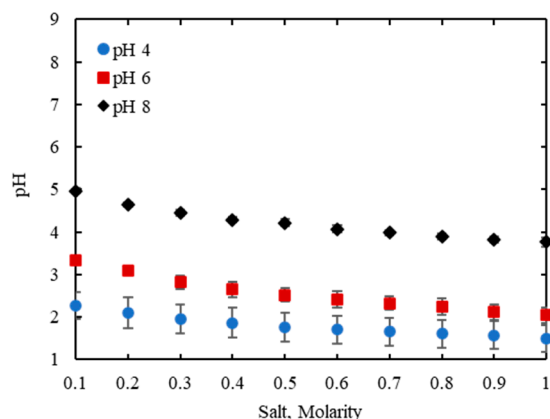

Figure 7. The pH values were calculated by the three-point calibration slope at aqueous pH 4, 6, and 8 with no salt or starch added (0 M). The error bar indicates the pH range for the viscous solutions with 2% or 4% starch added.
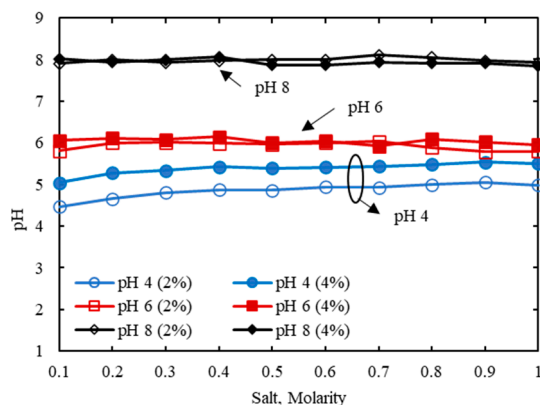

Figure 8. The pH values were calculated by the three-point calibrations conducted with aqueous pH 4, 6, and 8 solutions at individual NaCl concentrations. The viscosities of the 2% and 4% starch-added solutions correspond to 47 and 820 cP, respectively.

The effect of viscosity on the pH calibration error was particularly higher at pH 4, as indicated in Figure 8. The significant role of amylopectin matrices by starch in the high H^+ concentration created a higher potential difference. Since more ions could be constrained, the solution conductivity was lower compared to its aqueous case. As a result, higher pH errors occurred as viscosity increased. For example, the initial pH values of pH 4 changed to 4.46 and 5.04 at 2% and 4% starch, respectively, at the 0.1-M salt concentration. The larger pH errors at the more viscous solutions across all salt concentrations manifested the amylopectin matrix effect. Using a commercial pH meter, the results showed pH of 3.35 and 4.34 at 2% and 4% starch, respectively, for the 0.1-M salt case.

4.7. Specificity to pH

Based on the output potentials and calibrated pH levels in the different solutions, specificity to pH was performed to estimate the changes generated under ionic interferences. Potential deviation (ΔV) and pH deviation (ΔpH) were analyzed; ΔV in Figure 9 is the potential output difference between the aqueous and viscous solutions for a specific viscosity. There are five groups of viscosity data: four groups for starch from 1.17–820 cP and one group for agar at 2553 cP because the viscosity of 0.6% agar could not be measured because the solution became a gel-like solid (indicated by the † symbol).
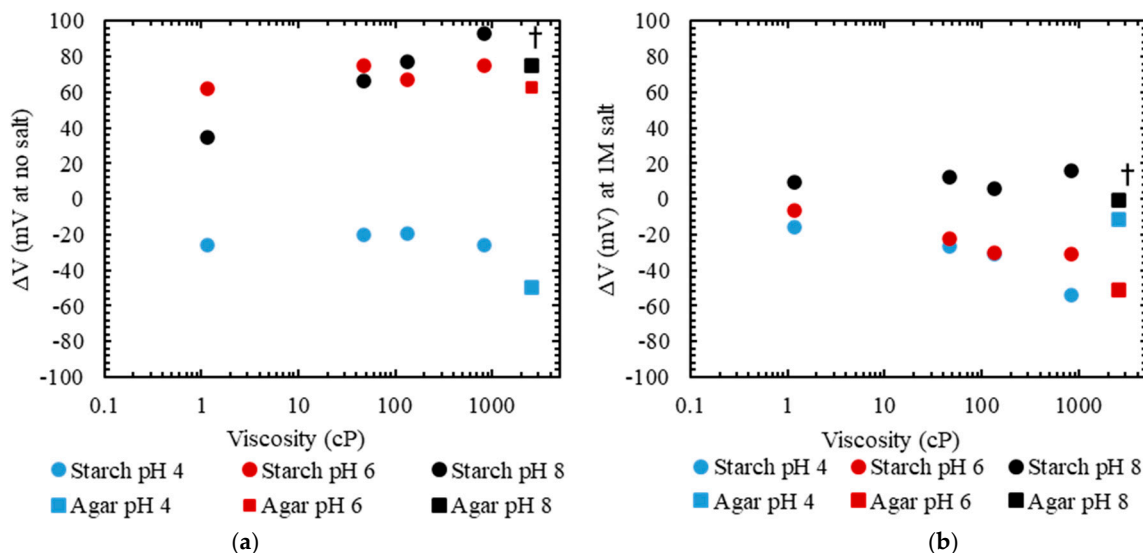

Figure 9. Potential change (ΔV) for viscous solutions with starch or agar added, at (**a**) no salt and (**b**) 1-M salt concentrations. Symbol †: only one group of ΔV data for agar at pH 4, 6, and 8.

Figure 9a shows the ΔV of starch and agar-added solutions at pH 4 (blue), pH 6 (red), and pH 8 (black) without salt added. Data above the zero point at the *y*-axis mean potential increases with increased viscosity, and data below the zero point mean potential decreases. The trends in output potential changes were previously indicated by red and purple arrows in Figures 4 and 6. Lower H$^+$ concentrations at pH 6 and 8 showed higher ΔV, whereas pH 4 remained relatively similar with increased viscosities. For the 1-M salt added cases, the pH 4 solutions experienced higher resistance from the amylopectin, which created higher ΔV, as shown in Figure 9b. Reduced ΔVs for pH 6 and 8 were due to the dominating conductivities of the added salt ions in low H$^+$ concentrations. Thus, potential deviations from viscous matrices were reduced. Overall, Figure 9 shows that ΔV tends to become higher with an increased viscosity if the conductivity is low in the solution.

Table 2 lists the worst ΔV for the starch cases (with concentrations of 1%, 2%, 3%, and 4% by weight) at no-salt, 0.1-M, and 1-M salt concentrations. The worst ΔV is defined as the highest potential deviation from the aqueous case due to viscosity. The values for no-salt and 1-M salt can be seen in Figure 9. Additional values for the 0.1-M salt cases were added in Table 2 to compare the ΔV with the 1-M case. The positive or negative signs indicate potential increase or decrease with an increasing viscosity, respectively. It was evident that ΔV became higher as viscosity increased, and ΔV became smaller once the salt was added. Similar ΔV values for adding salt of 0.1 M and 1 M showed smaller changes in potential outputs because the conductivities in the solutions were dominated by salt.

The pH deviation (ΔpH) is defined as the pH difference between the aqueous and viscous solutions. Aqueous solutions at pH 4, 6, and 8 at a specific salt concentration were used as the calibration standard. The pH values for the viscous solutions were calculated from their respective calibration slopes. Figure 10a shows the pH deviations measured by the IrO$_x$-Ag/AgCl electrode pairs for the 2% starch solutions that have a viscosity of

47 cP at different salt concentrations. The pH deviations with salt concentrations between 0.1 and 1 M were within the ranges of (0.3–0.6), (0.06–0.5), and (0.03–0.2) from their correct values of pH 4, 6, and 8, respectively. Figure 10b shows ΔpH measured by a commercial pH meter in the same conditions. The deviations were more predictable and confined to certain ranges for the IrO$_x$-Ag/AgCl electrode pair sensor with different salt concentrations. The commercial meter produced wider variations of errors, particularly for the alkaline cases.

Table 2. Worst ΔV (mV) for starch cases.

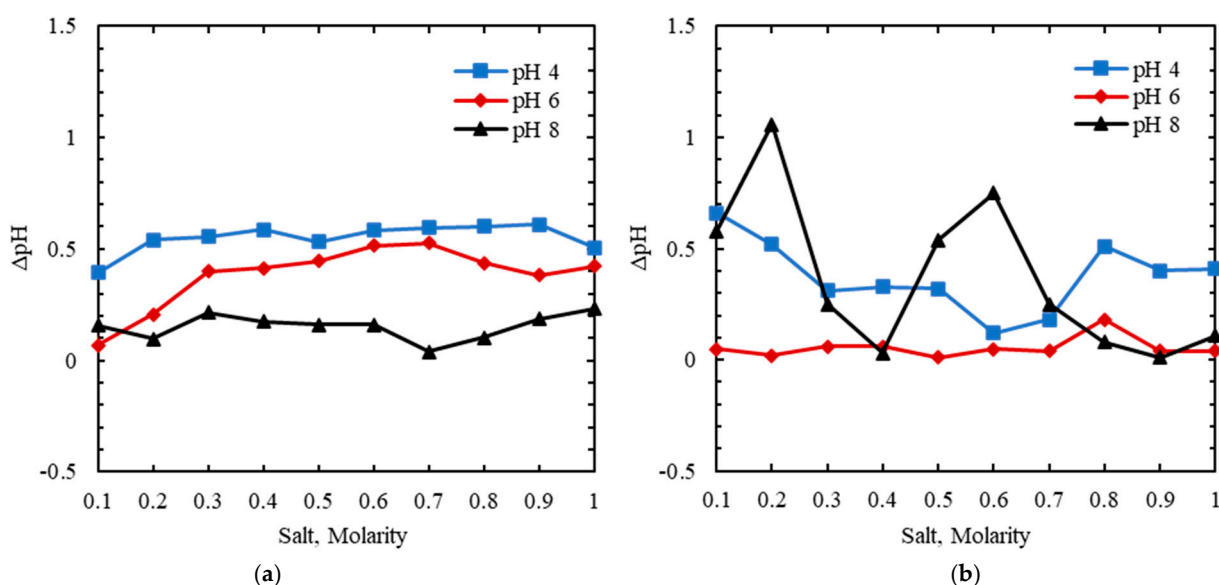|	1.17 cP	47 cP	135 cP	820 cP
No salt	62.1	74.7	77.5	92.9
0.1 M	−17.9	−21	−47.6	−52
1 M	−16	−26.5	−30.8	−53.6

(**a**)　　　　　　　　　　　　　　　　　　　　　　　　　(**b**)

Figure 10. The pH deviation (ΔpH) at the 2% starch solutions was measured by (**a**) the IrOx-Ag/AgCl pH sensor electrodes and (**b**) a commercial pH meter when 0.1–1 M NaCl was added.

Figure 11a shows the 4% starch cases with a viscosity of 820 cP. The pH deviations with the salt concentrations between 0.1 and 1 M were within the ranges of (0.9–1.1), (0.1–0.6), and (0.04–0.3) from their correct values of pH 4, 6, and 8, respectively. Figure 11b shows the results measured by a commercial meter. The planar electrodes once again provided better predictability for the pH values while the commercial meter obtained more diverse deviations. It is obvious that the pH deviation ranges became larger for more viscous solutions because the calibration slopes were conducted in respective aqueous solutions.

Although the deviation values in Figure 11a were higher, they were more confined within a range compared to Figure 11b. The diverse ΔpH detected by the commercial meter shown in Figures 10b and 11b for pH 8 were due to low H$^+$ concentrations and likely membrane clogging in the highly viscous environment.

In a typical human body, sodium concentration is around 0.1 M [50,51], and biofluids such as saliva, serum, and whole blood viscosities are in the range of 1–5 cP [52,53]. It is clear the pH deviations will not be as large as those shown in this paper when using our planar pH sensors in biomedical applications. This study covered wide ranges of viscosity and salt concentrations in order to study potential interference and calibration issues. Such issues may occur in the cases of food processing and preparation in which viscosities depend on processing methods. For example, the same ketchup can have different viscosities in different yield stresses during extrapolation, initiated flow, squeezing flow, or vane methods. The different viscosities may produce varied pH readings in different steps of processing

for the same ketchup. The viscosities of common food such as honey and sauce range between 23–578 cP [54,55]. Nectar-like and honey-like consistency food products added with a variety of thickening agents range between 51–350 and 351–1750 cP, respectively [56]. It was noted in [56] that there is variability in viscosity measurements within the same product line for thickening various liquids. Therefore, one would expect pH reading errors along the same product line when the solutions change viscosities. In this study, the viscosities covered the ranges of interest for the cases in [56].
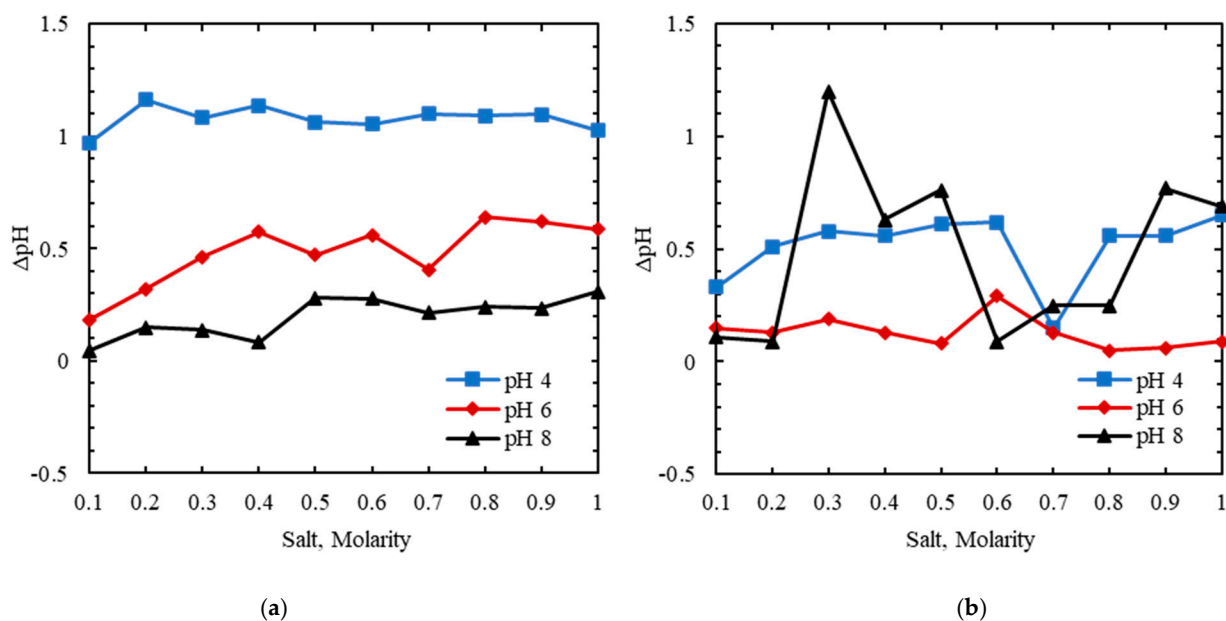

(**a**)   (**b**)

Figure 11. pH deviation (ΔpH) at the 4% starch concentration, measured by (**a**) the IrOx-Ag/AgCl pH sensor electrodes and (**b**) a commercial pH meter when 0.1–1 M NaCl was added.

5. Conclusions

This work investigated the effects of viscosity and salt interference on pH reading. A pair of planar IrO$_x$-Ag/AgCl electrodes deposited on a flexible polyimide substrate were used. The deposition of IrO$_x$ was conducted with sol-gel dipping and oxidation processes, while Ag/AgCl was screen printed. The cyclic voltammetry (CV) analysis was conducted at different pH levels. Super Nernstian response was achieved in aqueous solutions. Changes in Nernstian responses with salt additions showed that conductive ions created interference effects and potential shifts. The outcome showed that sensitivity was reduced.

The effects of viscosity and salt conductivity on sensor output potentials were studied. Viscous solutions were prepared with starch and agar as thickening agents. Different concentrations of salt were added to the aqueous and viscous solutions. Both factors were studied simultaneously and counteracting effects on potential outputs were found. The trends of potential shifts were examined and matched well for two different thickening agents. Two calibration methods for the potential-pH relationship were analyzed. It was clear that the calibration should be conducted with known salt concentrations to avoid large pH errors in solutions with high salt concentrations or high viscosity. Specificity to pH performance was investigated at two different viscosities with different salt concentrations and pH levels. The planar electrodes showed that the pH deviations were more predictable and confined within limited ranges compared to those measured with a commercial pH meter. It was also shown the pH deviations increased when viscosity increased. The results demonstrated potential uses of the planar flexible IrO$_x$-Ag/AgCl pH sensors in aqueous and viscous solutions, as well as the related issues of viscosity and salt interference. This investigation was conducted with wide ranges of viscosities and salt concentrations. It covers potential applications in diagnostics of human bodily fluids as well as cosmetic, food,

and pharmaceutical industries. The planar, flexible, and miniature features of the IrO_x-Ag/AgCl electrodes can operate without the concern for membrane clogging in viscous solutions. Thus, it can enable new applications.

References

1. Frant, M.S. How to Measure pH in Mixed and Nonaqueous solutions. *Today's Chem. Work* **1995**, 39–42.
2. Izutsu, K.; Yamamoto, H. Response of an Iridium Oxide pH-Sensor in Nonaqueous Solutions. Comparison with Other pH-Sensors. *Anal. Sci.* **1996**, *12*, 905–909. [CrossRef]
3. Pandey, P.C.; Singh, G. Tetraphenylborate doped polyaniline based novel pH sensor and solid-state urea biosensor. *Talanta* **2001**, *55*, 773–782. [CrossRef]
4. Samaranayake, C.P.; Sastry, S.K. In-situ pH measurement of selected liquid foods under high pressure. *Innov. Food Sci. Emerg. Technol.* **2013**, *17*, 22–26. [CrossRef]
5. Karastogianni, S.; Girousi, S.; Sotiropoulos, S. pH: Principles and measurement. *Encycl. Food Health* **2016**, *4*, 333–338.
6. Woolf, A.D.; Woolf, A.; Shaw, J.S. Nail primer cosmetics: Correlations between product pH and adequacy of labeling. *J. Toxicol. Clin.Toxicol.* **1999**, *37*, 827–832. [CrossRef]
7. Liudmyla, K.; Olena, C.; Nadiia, S. Chemical properties of Helix aspersa mucus as a component of cosmetics and pharmaceutical products. *Mater. Today Proc.* **2022**, *62*, 7650–7653. [CrossRef]
8. Traple, M.A.L.; Saviano, A.M.; Francisco, F.L.; Lourenço, F.R. Measurement uncertainty in pharmaceutical analysis and its application. *J. Pharm. Anal.* **2014**, *4*, 1–5. [CrossRef]
9. Mäder, K. Pharmaceutical applications of in vivo EPR. *Phys. Med. Biol.* **1998**, *43*, 1931. [CrossRef]
10. Artiola, J.F. Environmental chemical properties and processes. In *Environmental Monitoring and Characterization*; Elsevier Science: Amsterdam, The Netherlands, 2004; pp. 241–261.
11. Kurzweil, P. Metal Oxides and Ion-Exchanging Surfaces as pH Sensors in Liquids: State-of-the-Art and Outlook. *Sensors* **2009**, *9*, 4955–4985. [CrossRef]
12. Noh, J.; Park, S.; Boo, H.; Kim, H.C.; Chung, T.D. Nanoporous Platinum Solid-state Reference Electrode with Layer-by-layer Polyelectrolyte Junction for pH Sensing Chip. *Lab. A Chip* **2011**, *11*, 664–671. [CrossRef] [PubMed]
13. Suzuki, H.; Hiratsuka, A.; Sasaki, S.; Karube, I. Problems Associated with the Thin-film Ag/AgCl Reference Electrode and a Novel Structure with Improved Durability. *Sens. Actuators. B Chem.* **1998**, *46*, 104–113. [CrossRef]
14. Kim, T.Y.; Hong, S.A.; Yang, S. A Solid-State Thin-Film Ag/AgCl Reference Electrode Coated with Graphene Oxide and its Use in a pH Sensor. *Sensors* **2015**, *15*, 6469–6482. [CrossRef] [PubMed]
15. Manjakkal, L.; Szwagierczak, D.; Dahiya, R. Metal oxides based electrochemical pH sensors: Current progress and future perspectives. *Prog. Mater. Sci.* **2020**, *109*, 100635. [CrossRef]
16. Baur, J.E.; Spaine, T.W. Electrochemical deposition of iridium (IV) oxide from alkaline solutions of iridium (III) oxide. *J. Electroanal. Chem.* **1998**, *443*, 208–216. [CrossRef]
17. Kreider, K. Iridium Oxide Thin-Film Stability in High-temperature Corrosive Solutions. *Sensors Actuators B Chem.* **1991**, *5*, 165–169. [CrossRef]
18. Jang, H.; Lee, J. Iridium Oxide Fabrication and Application: A Review. *J. Energy Chem.* **2020**, *46*, 152–172. [CrossRef]
19. Bahrami, H.; Mirbozorgi, S.A.; Ameli, R.; Rusch, L.A.; Gosselin, B. Flexible, polarization-diverse UWB antennas for implantable neural recording systems. *IEEE Trans. Biomed. Circuits Syst.* **2015**, *10*, 38–48. [CrossRef]

20. Sun, Y.; Lacour, S.P.; Brooks, R.A.; Rushton, N.; Fawcett, J.; Cameron, R.E. Assessment of the biocompatibility of photosensitive polyimide for implantable medical device use. *J. Biomed. Mater. Res. Part A Off. J. Soc. Biomater. Jpn. Soc. Biomater. Aust. Soc. Biomater. Korean Soc. Biomater.* **2009**, *90*, 648–655. [CrossRef]

21. Shamma-Donoghue, S.A.; May, G.A.; Cotter, N.E.; White, R.L.; Simmons, F.B. Thin-film multielectrode arrays for a cochlear prosthesis. *IEEE Trans. Electron Devices* **1982**, *29*, 136–144. [CrossRef]

22. Klein, J.D.; Clauson, S.L.; Cogan, S.F. The influence of substrate bias on the morphology and charge capacity of rf-sputtered iridium oxide films. *J. Mater. Res.* **1989**, *4*, 1505–1510. [CrossRef]

23. Liu, D.; Yu, S.; Son, S.; Joo, S. Electrochemical performance of iridium oxide thin film for supercapacitor prepared by radio frequency magnetron sputtering method. *Ecs Trans.* **2008**, *16*, 103. [CrossRef]

24. Han, M.; McCreery, D.B. A new chronic neural probe with electroplated iridium oxide microelectrodes. In Proceedings of the 30th Annual International Conference of the IEEE Engineering in Medicine and Biology Society, Vancouver, BC, Canada, 20–25 August 2008; pp. 4220–4221.

25. Pikulski, M.; Gorski, W. Iridium-based electrocatalytic systems for the determination of insulin. *Anal. Chem.* **2000**, *72*, 2696–2702. [CrossRef] [PubMed]

26. Ohsaka, T.; Matsubara, Y.; Hirano, K.; Ohishi, T. Electroplating of iridium–cobalt alloy. *Trans. IMF* **2007**, *85*, 265–269. [CrossRef]

27. Chen, P.; Chen, Y.; Huang, C. Free-standing iridium oxide nanotube array for neural interface electrode applications. *Mater. Lett.* **2018**, *221*, 293–295. [CrossRef]

28. Chen, Y.; Chung, T.; Wu, P.; Chen, P. A cost-effective fabrication of iridium oxide films as biocompatible electrostimulation electrodes for neural interface applications. *J. Alloy. Compd.* **2017**, *692*, 339–345. [CrossRef]

29. Chawang, K.; Chou, S.; Bing, S.; Wu, P.; Chiao, J. Characterization of pH Sensors Based on Iridium Oxide and Gold Encapsulated Polypropylene Membranes. In Proceedings of the IEEE Sensors Conference, Sydney, Australia, 31 October–4 November 2021.

30. Marsh, P.; Huerta, M.; Le, T.; Yang, X.; Chiao, J.-C.; Cao, H. Wireless Iridium Oxide-Based pH Sensing Systems. In Proceedings of the IEEE Sensors Conference, New Delhi, India, 28–31 October 2018.

31. Nguyen, C.M.; Rao, S.; Yang, X.; Dubey, S.; Mays, J.; Cao, H.; Chiao, J.-C. Sol-gel Deposition of Iridium Oxide for Biomedical Micro-devices. *Sensors* **2015**, *15*, 4212–4228. [CrossRef] [PubMed]

32. Yang, X.; Chawang, K.; Chiao, J.-C. Wearable Iridium Oxide pH Sensors for Sweat pH Measurements. In Proceedings of the IEEE Sensors Conference, Montreal, QC, Canada, 28–31 October 2019.

33. Nguyen, C.M.; Huang, W.; Rao, S.; Cao, H.; Tata, U.; Chiao, M.; Chiao, J.-C. Sol-Gel Iridium Oxide-Based pH Sensor Array on Flexible Polyimide Substrate. *IEEE Sens. J.* **2013**, *13*, 3857–3864. [CrossRef]

34. Yang, X.; Chiao, J.-C. Integrated pH and Sodium Sensor Array Based on Iridium Oxide Film. In Proceedings of the IEEE Sensors Conference, New Delhi, India, 28–31 October 2018.

35. Huang, W.; Deb, S.; Seo, Y.; Rao, S.; Chiao, M.; Chiao, J.C. A Passive Radio-Frequency pH-Sensing Tag for Wireless Food-Quality Monitoring. *IEEE Sens. J.* **2011**, *12*, 487–495. [CrossRef]

36. Cao, H.; Rao, S.; Tang, S.; Tibbals, H.F.; Spechler, S.; Chiao, J. Batteryless Implantable Dual-Sensor Capsule for Esophageal Reflux Monitoring. *Gastrointest. Endosc.* **2013**, *77*, 649–653. [CrossRef]

37. Deb, S.; Tang, S.; Abell, T.L.; McLawhorn, T.; Huang, W.; Lahr, C.; To, S.F.; Easter, J.; Chiao, J. Development of Innovative Techniques for the Endoscopic Implantation and Securing of a Novel, Wireless, Miniature Gastrostimulator (with videos). *Gastrointest. Endosc.* **2012**, *76*, 179–184. [CrossRef] [PubMed]

38. Chawang, K.; Bing, S.; Chiao, J.-C. Investigation of pH Sensing in Viscous Salt-added Solution by Iridium Oxide Film. In Proceedings of the IEEE Sensors Conference, Dallas, TX, USA, 30 October–2 November 2022.

39. Huang, W.; Cao, H.; Deb, S.; Chiao, M.; Chiao, J.-C. A Flexible pH Sensor Based on the Iridium Oxide Sensing Film. *Sens. Actuators A Phys.* **2011**, *169*, 1–11. [CrossRef]

40. Yang, X.; Fu, T.; Kota, P.K.; Tjia, M.; Nguyen, C.M.; Chiao, J.-C. Lactate Sensors on Flexible Substrates. *Biosensors* **2016**, *6*, 48. [CrossRef] [PubMed]

41. Osaka, A.; Takatsuna, T.; Miura, Y. Iridium oxide films via sol-gel processing. *J. Non Cryst. Solids* **1994**, *178*, 313–319. [CrossRef]

42. Olthuis, W.; Robben, M.; Bergveld, P.; Bos, M.; van der Linden, W.E. pH Sensor Properties of Electrochemically Grown Iridium Oxide. *Sensors Actuators B Chem.* **1990**, *2*, 247–256. [CrossRef]

43. Chou, S.C.; Hsieh, Y.C.; Cheang, W.H.; Sun, B.Y.; Chu, C.Y.; Chen, S.Y.; Chiao, J.C.; Wu, P.W. A flexible IrO2 membrane for pH sensing. *Sci. Rep.* **2022**, *12*, 11712. [CrossRef]

44. Wang, G.; Zhou, M.; Goettel, J.T.; Schrobilgen, G.J.; Su, J.; Li, J. Identification of an iridium-containing compound with a formal oxidation state of IX. *Nature* **2014**, *514*, 475–477. [CrossRef]

45. Bause, S.; Decker, M.; Gerlach, F.; Näther, J.; Köster, F.; Neubauer, P.; Vonau, W. Development of an iridium-based pH sensor for bioanalytical applications. *J. Solid State Electrochem.* **2018**, *22*, 51–60. [CrossRef]

46. Hernandez-Jaimes, C.; Lobato-Calleros, C.; Sosa, E.; Bello-Pérez, L.A.; Vernon-Carter, E.J.; Alvarez-Ramirez, J. Electrochemical Characterization of Gelatinized Starch Dispersions: Voltammetry and Electrochemical Impedance Spectroscopy on Platinum Surface. *Carbohydr. Polym.* **2015**, *124*, 8–16. [CrossRef]

47. Rajeswari, A.; Gopi, S.; Christy, E.J.S.; Jayaraj, K.; Pius, A. Current research on the blends of chitosan as new biomaterials. In *Handbook of Chitin and Chitosan*; Elsevier: Amsterdam, The Netherlands, 2020; pp. 247–283.

48. Bementa, E.; Rajan, M.A.J.; Gnanadass, E.S. Effect of Prolonged Duration of Gelatinization in Starch and Incorporation with Potassium Iodide on the Enhancement of Ionic Conductivity. *Polym.-Plast. Technol. Eng.* **2017**, *56*, 1632–1645. [CrossRef]
49. Bennett, D. NaCl Doping and the Conductivity of Agar Phantoms. *Mater. Sci. Eng. C* **2011**, *31*, 494–498. [CrossRef]
50. Strazzullo, P.; Leclercq, C. Sodium1. *Adv. Nutr. Bethesda Md.* **2014**, *5*, 188–190. [CrossRef] [PubMed]
51. Pohl, H.R.; Wheeler, J.S.; Murray, H.E. Sodium and potassium in health and disease. In *Interrelations between Essential Metal Ions and Human Diseases*; Springer: Berlin/Heidelberg, Germany, 2013; pp. 29–47.
52. International Association for Dental Research. Available online: https://iadr.abstractarchives.com/abstract/18iags-2954851/relationship-of-saliva-viscosity-and-ph-at-resting-and-stimulation (accessed on 7 September 2022).
53. Piagnerelli, M.; Boudjeltia, K.Z.; Vanhaeverbeek, M.; Vincent, L.-J. Physiological Reviews. In *Applied Physiology in Intensive Care Medicine*, 2nd ed.; Pinsky, M.R., Brochard, L., Mancebo, J., Hedenstierna, G., Eds.; Springer: Berlin/Heidelberg, Germany, 2006; pp. 273–282.
54. Yanniotis, S.; Skaltsi, S.; Karaburnioti, S. Effect of moisture content on the viscosity of honey at different temperatures. *J. Food Eng.* **2006**, *72*, 372–377. [CrossRef]
55. Kim, H. The mineral contents, viscosity and sensory characteristics of demi-glace sauce according to the varying quantity of omija added. *J. Korean Soc. Food Cult.* **2004**, *19*, 667–677.
56. Garcia, J.M.; Chambers, E.; Matta, Z.; Clark, M. Viscosity measurements of nectar-and honey-thick liquids: Product, liquid, and time comparisons. *Dysphagia* **2005**, *20*, 325–335. [CrossRef]